Submitted to ACS APPLIED MATERIALS & INTERFACES

Tunable Electrical Properties of Embossed, Cellulose-based Paper for Skin-like Sensing

*Tongfen Liang[1‡], Xiyue Zou[1‡], Ramendra Kishor Pal[1], Jingjin Xie[1], Maame Konadu Assasie-Gyimah[1], Jiaqi Liu[1], Weijian Guo[1], Chuyang Chen[1], Max Tenorio[1], Daniel Sullivan[1], Anna Root[2], Paul Stansel[3], Anne Q. McKeown[4], George J. Weng[1], William Sampson[5], Assimina Pelegri[1], and Aaron D. Mazzeo[1],**

[1]Department of Mechanical and Aerospace Engineering, Rutgers University, Piscataway, NJ 08854, USA

[2]School of Arts and Sciences, Rutgers University, New Brunswick, NJ 08901, USA

[3]MPS Systems, 490 Rollstone Road, Fitchburg, MA 01420, USA

[4]Mason Gross School of Arts, Rutgers University, New Brunswick, NJ 08901, USA

[5]School of Materials, The University of Manchester, Oxford Rd, Manchester, M13 9PL, UK

*Author to whom correspondence should be addressed. Electronic mail: aaron.mazzeo@rutgers.edu

KEYWORDS: piezoresistive paper, three-phase composite, tunable conductivity, embossing, skin-like sensing

ABSTRACT

This article describes a process of fabricating highly porous paper from cellulosic fibers and carbon black (CB) with tunable conductivity. By embossing such paper, its porosity decreases while its conductivity increases. Tuning the porosity of composite paper alters the magnitude and trend of conductivity over a spectrum of concentrations of conductive particles. The largest increase in conductivity from 8.38×10^{-6} S/m to 2.5×10^{-3} S/m by a factor of ~300 occurred at a percolation threshold of 3.8 wt% (or 0.36 vol%) with the composite paper plastically compressed by 410 MPa, which causes a decrease of porosity from 88% to 42% on average. Our composite paper showed stable piezoresistive responses within a broad pressure range from 1 kPa up to 5.5 MPa for 800 cycles. The piezoresistive sensitivities of the composite paper were concentration-dependent and decreased with pressure. Composite paper with 7.5 wt% CB had sensitivities of -0.514 kPa^{-1} over applied pressures ranging from 1 kPa to 50 kPa and -0.215 kPa^{-1} from 1 kPa to 250 kPa. This piezoresistive paper with embossed patterns enabled touch sensing and detection of damage from darts and punches. Understanding the percolation behavior of three-phase composites (cellulosic fibers/conductive particles/air) and their response to damage, pressure, and processing conditions has the potential to enable scalable applications in prosthetics and robotics, haptic feedback, or structural health monitoring on expansive surfaces of buildings and vehicles.

1. Introduction

Papertronics, or paper-based electronics, are emerging as flexible, lightweight, recyclable, and low-cost options for advanced mechanical, chemical, and electrical sensing. The broad range of capabilities of papertronics is promising in applications such as tactile/pressure sensors, transistors, energy-storage devices, memory devices, electrochemical analysis, triboelectric nanogenerators, and circuits.[1–16] Recently, skin-like sensing of papertronics has shown an integrated ability to detect touch, strain, temperature, pH, humidity, and force/pressure, which may be useful for wearable sensors, human-machine interfaces, structural health monitoring, and prosthetics.[17–20] Previous efforts on paper-based skins have employed paper as a passive platform to support conductive coatings to detect strain, touch, and environmental factors (e.g., pH, temperature, humidity).[18,20–23] Some efforts also demonstrated an approach to measuring force/pressure through capacitive measurements with a piece of insulative, porous material (e.g., microfibril wipe or sponge).[18] In contrast to these examples of *electronics on paper*, piezoresistive sheets with embedded conductive particles (such as carbon black (CB), carbon nanotubes (CNTs), graphene, gold nanowires, and silver nanowires) detected force/pressure.[24,25,4,26–28]

In this study, we fabricated piezoresistive paper containing carbon black and then tuned its electrical properties through compression. Furthermore, we patterned paper through selective embossing to customize the size/functionality of the sensors. This embossing approach offers an alternative, simple approach to fabricating scalable, skin-like sensors. As a demonstration, we embossed samples of our composite paper with patterns to detect both human touch and damage from darts.

Past studies tuned the conductivity of composite paper by varying the concentration of conductive particles while keeping bulk porosity constant.[29–31] In contrast, Wang and Drzal showed that hot-pressing reduced the porosity of hybrid paper made by cellulose nanofibrils

and graphene nanoplatelets, which increased the conductivity of paper by up to 50 fold.[32] However, few studies have explained how composite paper behaves in terms of filler concentration and bulk porosity, and this study manipulates both of these factors. We relate theoretical models of percolation from the literature to our experimental characterization of conductivity in three-phase (cellulosic fibers, air, and conductive fillers), fibrous nanocomposites.

To fabricate highly porous and uniform conductive paper, we've modified a water-efficient foam-laying process for papermaking,[29,33,34] as shown in Figure 1. The foam-laying process uses a foaming agent, or surfactant, to make homogeneous, porous composite paper. Prior uses of surfactant in dispersing carbonaceous particles avoid foaming or bubbling by ultrasonication or by adding antifoaming agents.[35–37] However, the surfactant in our foam-laying process helps lower the surface tension of the aqueous suspension containing cellulosic fibers. Then, the suspension foams when mixed with air.[38] The bubbles in the foam separate and redistribute fibers in an enlarged volume, which also prevents flocculation.[39] Vacuum filtration densifies and drains out the bubbles, which helps to form a porous mat of cellulose fibers after drying (Figure 2a, S1). We emboss the samples at room temperature for electrical characterization.

2. Results and Discussion

2.1 Morphology change of composite paper before and after embossing

Figures 2b-g and Figure S2 show scanning electron microscope (SEM) images of fibrous network. The morphology of the composite paper changed significantly after embossing with decreased porosity. Before embossing, the fibers were sparsely arranged with few contacts per fiber. After embossing, the gaps between fibers became small and even negligible, which narrowed the gaps between the CB particles. Most fibers became flat with an increased top-down, cross-sectional area. Figure S3 shows magnified images of the surface of

fibers. As the filler concentration increased, the CB on the fibers evolved from sparse loading to dense loading, which coarsened the fiber surface.

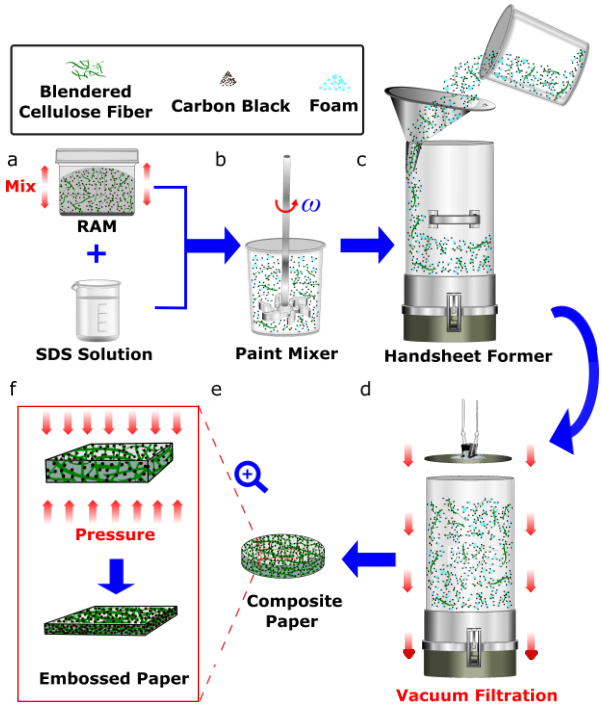

Figure 1. Schematic diagram of the process to fabricate composite paper by the foam-laying method and to tune its porosity by embossing. (a) Mixing cellulose fibers and carbon black in water by a Resonant Acoustic Mixer (RAM). (b) Generating foam by a mechanical mixer agitating the aqueous solution of carbon black, fibers, and sodium dodecyl sulfate (SDS). (c) Decanting the foam into the handsheet former through a funnel. (d) Removing bubbles by vacuum filtration with a polished steel plate covering the foam. (e) Composite paper out of a drying ring. (f) Embossing a small sample out of the composite paper.

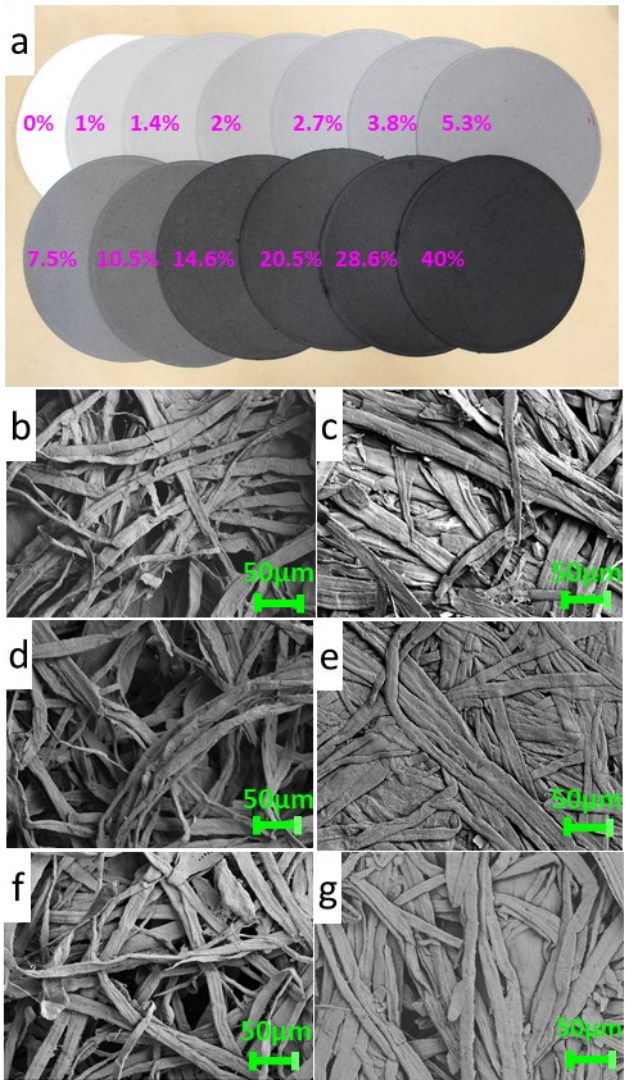

Figure 2. (a) Picture of fabricated composite paper at the concentration of CB from 0 wt% to 40 wt%. (b) - (g) are SEM images of composite paper. (b) and (c) are of 0 wt% CB before embossing and after embossing, respectively. (d) and (e) are of 3.8 wt% before embossing and after embossing, respectively. (f) and (g) are of 10.5 wt% before embossing and after embossing, respectively. (b) has brightness increased by 20% and contrast by 40%, (c) has brightness increased by 20%, (d) has brightness increased by 20% and contrast decreased by 20%, and (f) has brightness increased by 40%.

2.2 AC conductivity of composite paper by admittance/impedance spectroscopy

Figure S4a details the impedance-frequency response of composite paper at low concentrations of CB (1 wt%, 1.4 wt%, 2 wt%, and 2.7 wt%). These samples exhibited indistinguishable electrical impedance over the AC frequencies before and after compression, behaving like capacitors with high magnitudes of impedance and negative phase angles (close to -90°). Figure 3a illustrates the impedance-frequency response of samples at 3.8 wt% and 5.3 wt% concentrations. Starting from 3.8 wt%, the impedances of the samples were statistically distinct from each other before and after compression. The *p*-value at 10 kHz was less than 4.2×10^{-5} between uncompressed samples and less than 4.4×10^{-5} between compressed samples, both significantly lower than 0.05. After compression, the magnitude of impedance decreased, while the phase increased. The magnitude of the compressed samples with 3.8 wt% CB approximated that of the uncompressed samples with 5.3 wt% CB. Figures S5 and S6 show the impedance of characterized samples with high concentrations of CB from 7.5 wt%. For samples from 14.6 wt% and above, the phases of the samples increased to approach 0°, behaving like resistive elements.

Table S1 shows the conductivities of our composite paper. For both uncompressed and compressed samples, the conductivities increased nonlinearly with the concentration of CB, as presented in Figure 3b. The conductivity was low before rapidly increasing in the vicinity of 3.8 wt%; then it gradually increased at high concentrations of CB. For composite paper at each concentration of CB, its corresponding conductivity shifted upward after the embossing process. The greatest shift occurred at 3.8 wt% (or 0.36 vol%, calculated by Eq. (S1) in the SI): its conductivity increased by a factor of 298, i.e., from 8.38×10^{-6} S/m to 2.5×10^{-3} S/m. This increase in conductivity was concurrent with a decrease in porosity from 88% to 42.4% on average by compression. The compressed, densely packed CB-coated fibers formed more electrically conductive paths than those with higher porosity at the same concentration of CB.

Composite paper with 40 wt% CB achieves conductivities of 27.7 S/m before compression and 122 S/m after compression, which are comparable with other works (Table S2).

One can view paper composites as "an effective medium": an electrical network of resistances/impedance, or a lattice of sites and bonds. Within this network, increasing the volumetric fraction of conductive fillers or particles can lead to dramatic changes in electrical conductivities, dielectric permittivity, and mechanical properties of electronic composites.[40] According to the percolation theory, there is a critical concentration of particles at which the material transitions from low conductivity to significantly high conductivity, which is the electrical percolation threshold. This transition follows the universal scaling law, as shown in Eq. (1).

$$\sigma \propto \begin{cases} \sigma_f (f - f_c)^t & f > f_c \\ \sigma_m (f_c - f)^s & f < f_c \\ \sigma_m^u \sigma_f^{1-u} & f \approx f_c \end{cases} \quad (1)$$

where $\sigma, \sigma_f, \sigma_m$ are the conductivities of the composite, fillers, and the matrix, respectively; f is the volumetric fraction of the fillers; f_c is at the percolation threshold; *t*, *s*, and *u* are critical exponents for either two-dimensional (2D) or three-dimensional (3D) object-based morphologies. For 2D morphologies, $t = 1.1 - 1.3, s = 1.1 - 1.3$; for 3D morphologies, $t = 1.6 - 2.0, s = 0.7 - 1.0;\ u = t/(t+s)$.[41,42] According to Eq. (1), the *log(σ)* is proportional to the adjusted CB concentration *log(f-f$_c$)* in the region above the percolation threshold. Linear regression analysis confirms the percolation threshold to be 3.8 wt%. Deduced from the slopes of the fitting curves in Figure 3c, the critical exponents *t* for samples before and after embossing are 3.6 and 2.47, respectively. Further analysis of the slopes is available in Figure S7. Similarly, we obtained exponents *s* (0.05 before compression and 0.15 after compression) in Figure S8.

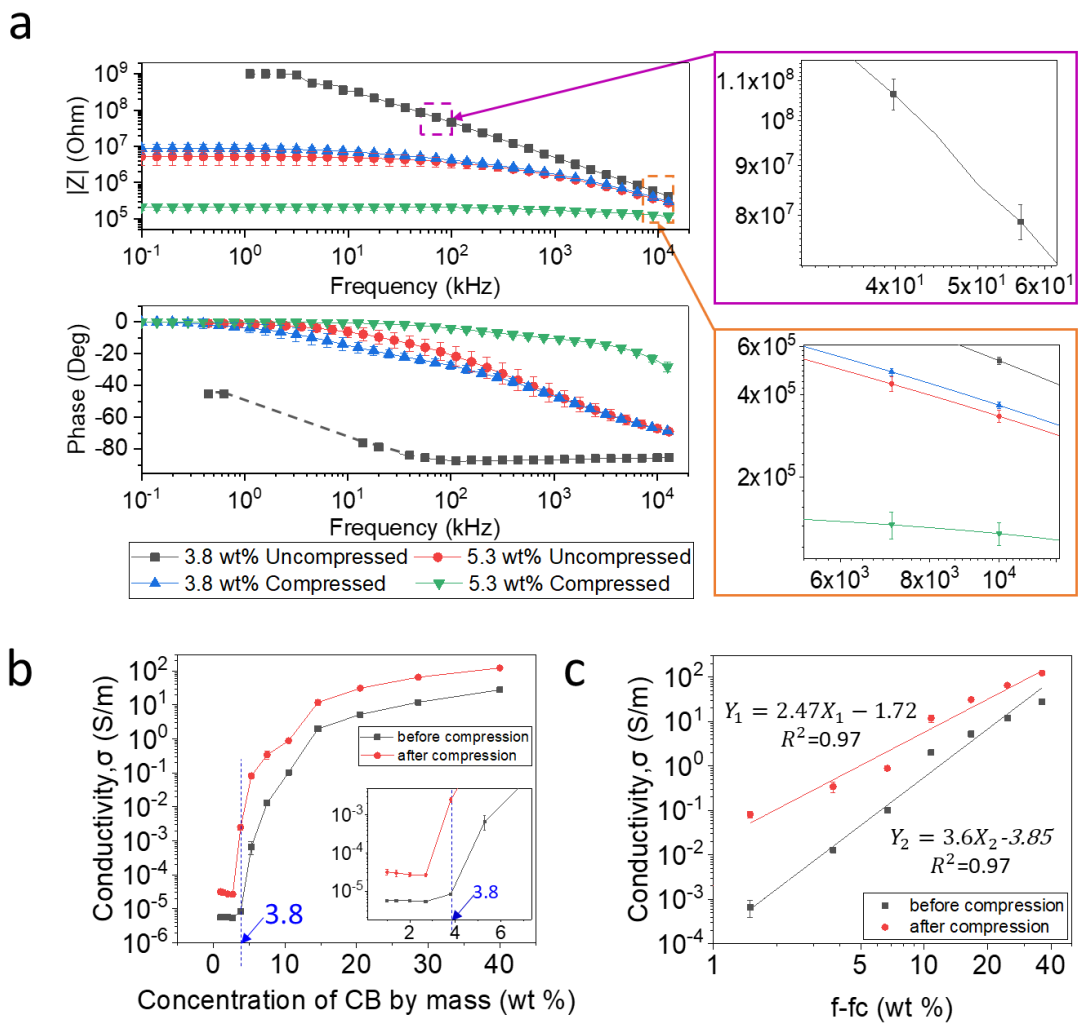

Figure 3. (a) The frequency response of impedance (magnitude and phase) of composite paper at CB concentrations of 3.8 wt% and 5.3 wt% before and after compression (8 repetitive samples). The curves are skipping 3 points for clarity. For the phase of 3.8 wt%, there were only some measurable sporadic values at low frequencies. (θ_Z= -45° at frequencies of 446 Hz, 562 Hz, and 630 Hz, θ_Z= -75.96° at 14.125 kHz.) The dashed line shows interpolated phases of 3.8 wt% at the frequencies from 1 kHz to 10 kHz. The data set of 3.8 wt% has one outlier removed. The zoomed-in figures show the error bars. (b) The conductivities of samples over the concentration (weight fraction) of CB at the excitation frequency of 10 kHz. The inset shows the conductivities at low concentrations of CB. (c) Curve fitting of the log-log plot of

conductivity over the adjusted concentration of CB for samples above the percolation threshold ($f > f_c$, f_c=3.8 wt%) .

The critical exponents of our composite paper are different from the universal values in the literature. Our composite paper is a three-phase material with cellulosic fibers, CB fillers, and open pockets of air, in which the exponents *t* (3.6 before embossing, 2.47 after embossing) exceed the typical range of 1.6-2 for 3D morphologies of two-phase materials. The exponents *s* (0.05 before embossing, 0.15 after embossing) are significantly lower than the literature values (0.7-1.0) for two-phase materials. Our non-universal values of exponents might occur due to frequent tunneling events, contact resistance, or structural imperfections in the conductive media (like the Swiss cheese model).[43,44]

2.3 Piezoresistive response of composite paper

Figure 4 shows the piezoresistive response of composite paper (7.5 wt%, 10.5 wt%, 20.5 wt%) under normal cyclic pressure. For the 10-cycle test, as shown in Figure 4a, our composite paper showed stabilized responses to pressure after the first cycle,[45] and exhibited low hysteresis in consecutive loading-unloading cycles. The composite paper displayed negative resistance variation with pressure within a broad pressure range from 1 kPa up to 5.5 MPa (Figure S9ab), which may apply for gentle touch (>10 kPa) and other human dynamic motions.[28,46] In the pressure-response curves of Figure 4a, *S1* and *S2* denote the pressure sensitivities ($S=\delta(\Delta R/R0)/\delta P$, relative resistance change divided by pressure change) of composite paper upon loading in the low-pressure range (1 kPa−250 kPa) and the high-pressure range (250 kPa−up to 5.5 MPa), respectively. The piezoresistive sensitivities of our composite paper decreased with pressure, which is due to the increasing elastic resistance with compression.[47]

The composite paper showed concentration-dependent piezoresistive sensitivity. For the loading state in the low-pressure range, the sensitivities *S1* to pressure of the composite

paper diminished, going from -0.215 kPa^{-1} to -0.035 kPa^{-1}, as the concentration of CB increased from 7.5 wt% to 20.5 wt%. In the high-pressure range, the sensitivities *S2* of the composite paper increased with the concentration of CB but remained comparatively small, with values up to $-0.004\ kPa^{-1}$. For the unloading state, the sensitivities show similar trends as those upon loading (Table S3). Although our composite paper shows limited sensitivity in these broad ranges, composite paper with 7.5 wt% CB achieves $-0.514\ kPa^{-1}$ at the loading state and $-0.585\ kPa^{-1}$ at the unloading state over applied pressures ranging from 1 kPa to 50 kPa (Table S4 and Figure S9c), which exceeds the sensitivities of some graphene-based pressure sensors in this pressure range.[4,48] Incorporating other nanoparticles in this framework can potentially bring out highly sensitive piezoresistive sensors as Table S5 suggests.

The dependence of piezoresistive sensitivities on the CB concentration of the composite is likely attributable to tunneling effects between CB particles. According to Wang et al., the resistance of CB-rubber composite depends on the resistance between CB particles, which form conductive paths mainly by tunnel currents; compressing such two-phase composite changes the number of effective conductive paths and the electrical resistance of a single effective conductive path.[49,50] In the low-pressure range, more conductive paths form under compression for the low-concentration CB composites (LCBC) than the high-concentration CB composites (HCBC). Furthermore, due to the greater change of gap/distance between CB particles, the resistance of single effective conductive paths of LCBC decreases more than that of HCBC.[51] Similarly, these two reasons may contribute to the higher piezoresistive sensitivity of our three-phase LCBC than HCBC in the low-pressure range. However, in the high-pressure range, compared with HCBC, LCBC could become more susceptible to the destruction of conductive paths caused by transverse slippage of CB, which decreases the piezoresistive sensitivity.[52]

Our composite paper exhibited repeatable piezoresistivity. Composite paper with 7.5 wt% CB showed stable responses during 800 cycles of compression up to 5.5 MPa

(Figure 4b). The relative changes of resistance in the low-pressure range were slightly positive in the first few cycles, gradually dropped to negative values, and stabilized starting from the 40th cycle. Figure 4c and 4d show the magnified cycles at the beginning and at the end of the compression, where the variations of relative change in resistance are neglectable.

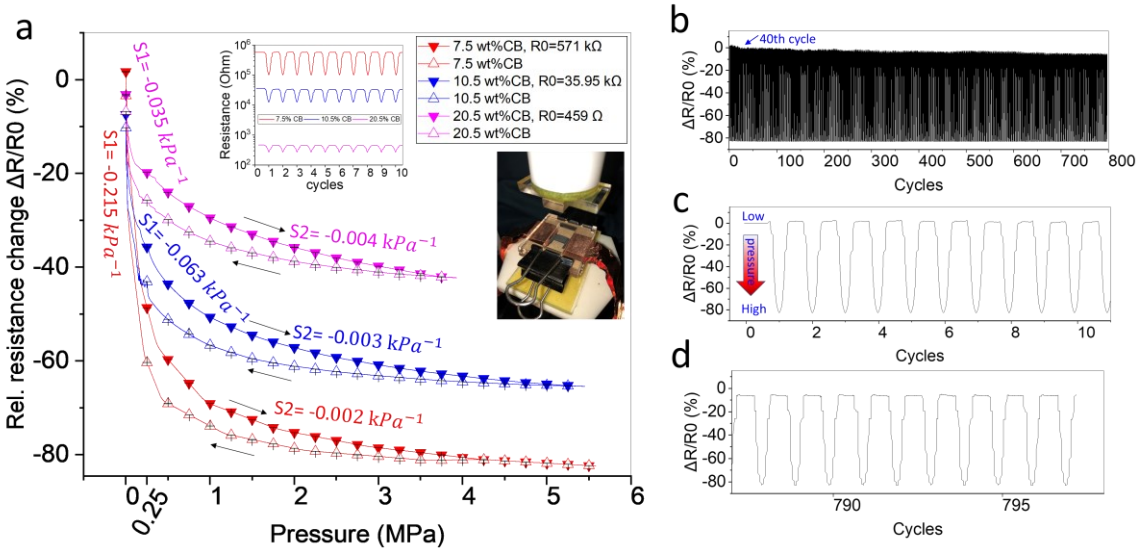

Figure 4. (a) Pressure-response curves for composite paper with the mean values and standard deviations based on 9 cycles after 1st-cycle stabilization. For clarity, we plot points at an interval of 0.25 MPa. The right arrows denote loading and left arrows unloading. *S1* denotes the sensitivity between 0.001MPa−0.25 MPa, *S2* denotes the sensitivity after 0.25 MPa. We only label the sensitivities of the loading state here. Composite paper with 7.5 wt% CB had the steepest slope or the highest pressure sensitivity (−0.215 kPa^{-1}), which was six times larger than that of the 20.5 wt% composite (−0.035 kPa^{-1}). The inset figure shows the resistance over 10 cycles; the inset photo shows the setup of the compression test. (b) The relative change of resistance of 7.5 wt% CB over nearly 800 cycles. (c) The relative change of resistance of 7.5 wt% CB over the first 10 cycles of (b). (d) The relative change of resistance of 7.5 wt% CB over the last 10 cycles of (b).

2.4 Demonstration 1: A skin-like touch sensor over a curved surface

To demonstrate the feasibility of composite paper in skin-like sensing, we created a skin-like tactile sensor by embossing composite paper with patterned molds to form conductive traces and regions. The compressed/recessed areas of the paper exhibited higher conductivity than the uncompressed regions. Figures 5a-f show a skin-like sensor made of composite paper (diameter of 8 cm, 21.6 wt% CB), which had embossed patterns forming four active electrodes and a central common ground. The common ground had four branches; each branch extended into one electrode to form a capacitive sensing button. The capacitance of these sensing buttons changed when a finger bridged the internal gap (i.e., the uncompressed region of the button). The embossed regions with different porosities divided the composite paper, which helped it conform to curved surfaces. To keep the uncompressed regions from collapsing by human touch, we supported the sensing disk by a cardboard layer with reliefs (Figures 5d,e). We then wrapped the disk around a cylindrical cardboard sleeve to form a skin-like sensing pad.

Repetitively touching each button on the sensing pad caused steady increases in capacitance, as shown in Figure 5g and Video S1. There was some crosstalk between buttons as they connected through the uncompressed regions (not completely electrically insulating). Touching one button leads to a change in the overall impedance of the sensing pad, which triggered small responses from other buttons as well. Among the four buttons, Button 4 exhibited the highest increase in capacitance. However, touching the uncompressed regions did not generate significant changes in capacitance.

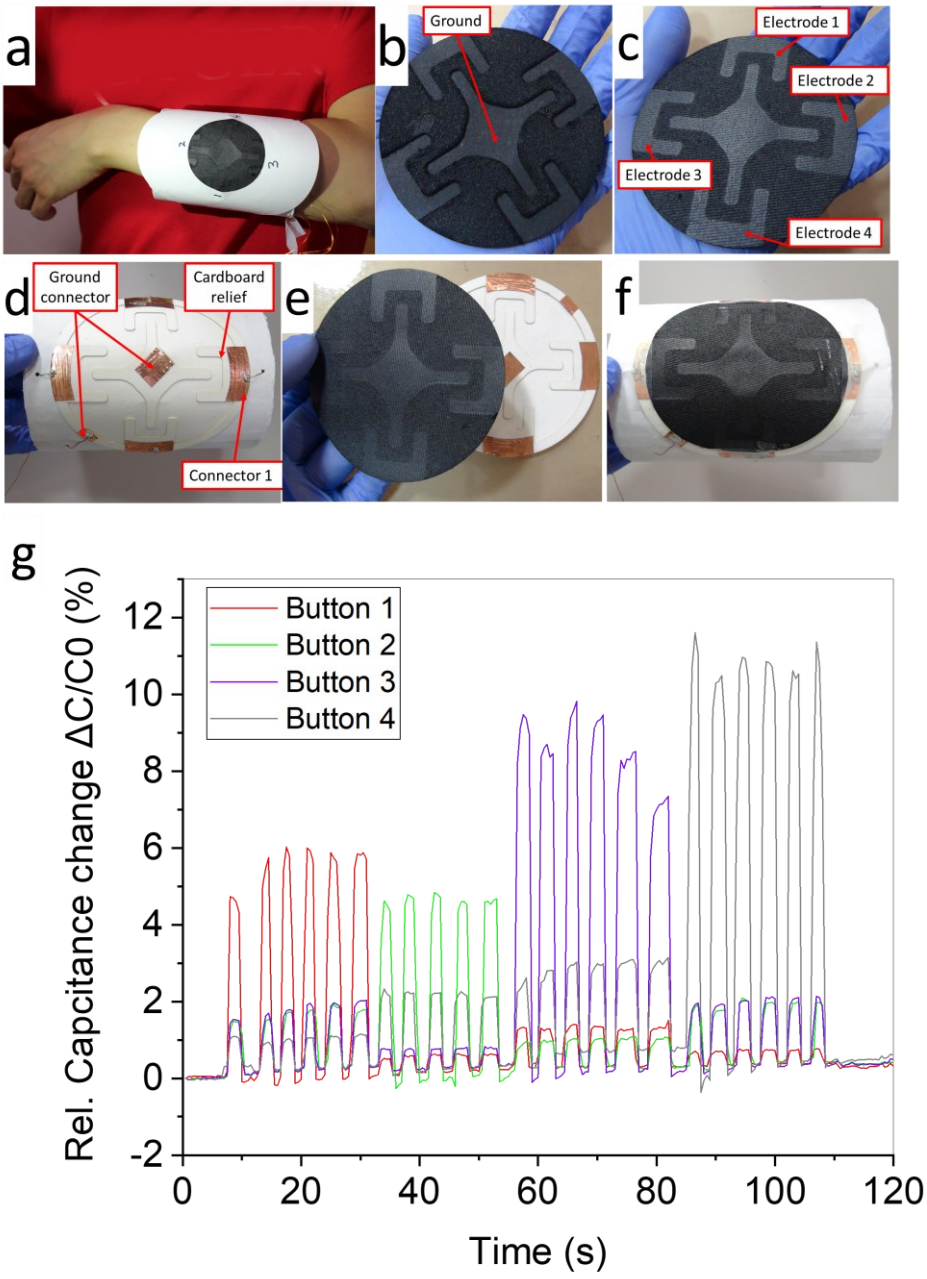

Figure 5. A skin-like sensor made of composite paper (21.6 wt% CB) with embossed patterns. (a) Picture of a person wearing a cylindrical cardboard sleeve with the skin-like sensing pad covering on top. (b) The front of the embossed composite paper. (c) The flat back of the embossed composite paper. (d) The supporting layers with relieves made of cardboard and electrodes made of copper tape. (e) and (f) show the assembly of the embossed composite paper on top of the cardboard. (g) Relative changes in measured capacitance of the skin-like sensors by human touch.

2.5 Demonstration 2: A dartboard

To investigate the response of the composite paper to damage, we designed a dartboard with compressed composite paper (21.6 wt% CB). The dartboard consisted of five regions, Rings 1 - 4 and a bullseye (Figure S10a). We shot/dropped darts with metal tips from above the dartboard through a guiding tube (Figure S10b) into the five regions and measured the corresponding changes in resistance. Figures 6a,b and Video S2 illustrate that the resistance of each region increased with damage from the darts. The bullseye displayed the most significant increase in resistance nearly after every shot except the third one, which might be a result of its smaller area compared with the surrounding rings. The third shot at the bullseye overlapped the holes of earlier shots so that it only induced a slight increase in resistance.

The change in resistance of the composite paper reflects the level of damage done to the designated regions by the darts. Damaging the interconnected network of CB-loaded fibers interrupted its electrical functionality. Figure S11 depicts the average increase in resistance for the rings due to the first and second effective hits. The change in resistance caused by the second effective hit nearly doubled the value of the first ones. For Ring 2, we regarded the second and fourth shots as the first and second “effective hits”, respectively; the first and third shots missed the region, but they caused small fluctuations in the resistance due to their substantial impact on the dartboard; the first shot lit the LED on the MATLAB graphic user interface (GUI), due to the low threshold setting of the program. Numerical simulation confirms that the resistance of the sheet increases linearly with the number of holes caused by darts, showing small variations with the distribution of the darts (Figures S12). From the simulation, targeted substrates with a smaller area will experience larger changes in resistance by darts than those with a larger area (Figure S13), which explains why the bullseye has a more significant change in resistance than the surrounding rings.

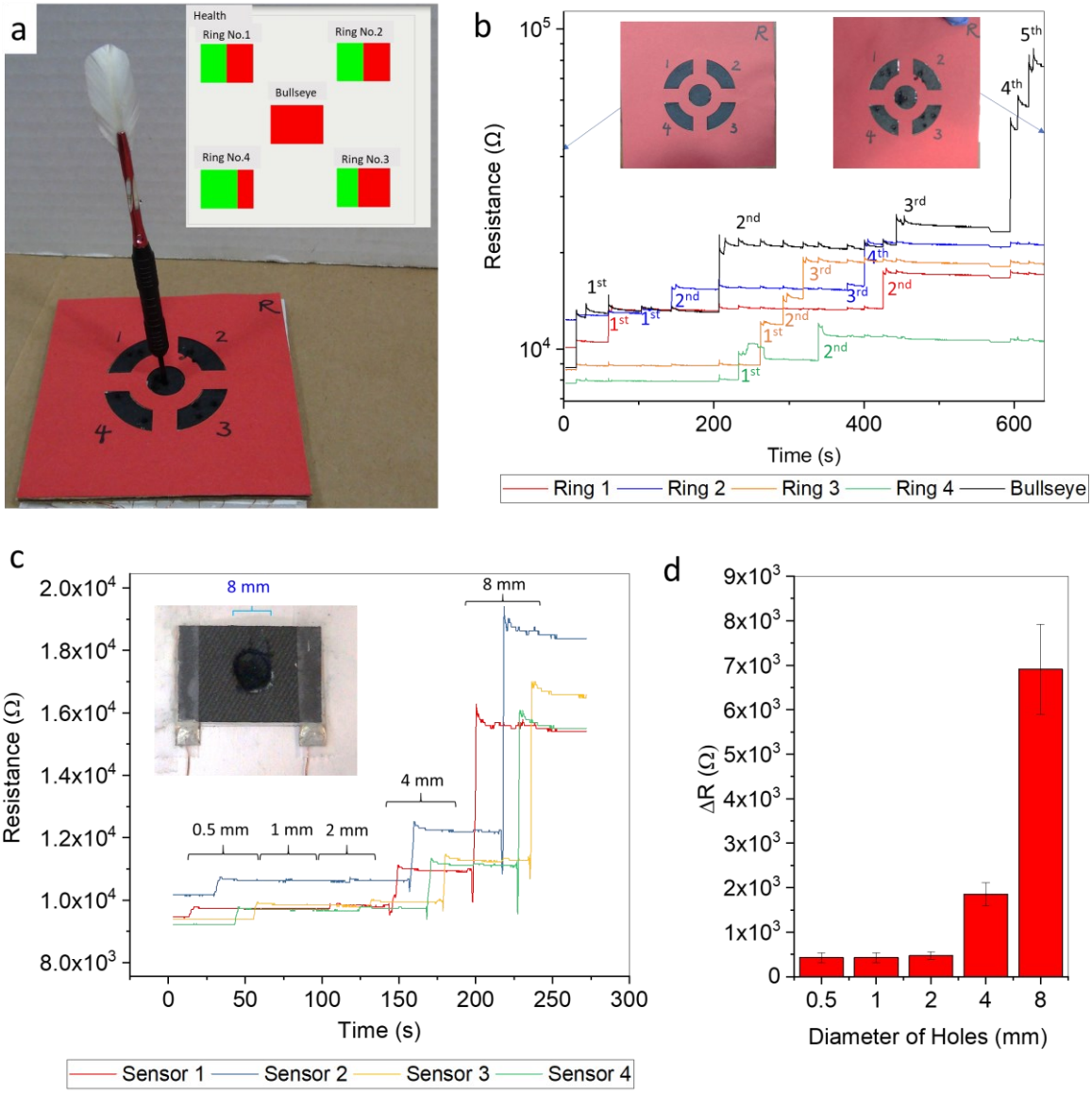

Figure 6. Test of damage on the composite paper. (a) Picture of a dart with a mass of 20 g hitting the bullseye. The inset shows the MATLAB GUI. (b) Resistance changes of the dartboard when hit with darts in different regions. The darts stay in the dartboard for 7 seconds on average before removal. The inset photos show the dartboard before and after shooting. (c) Changes in resistance of the four sensors punctured by holes of different diameters (0.5 mm, 1 mm, 2 mm, 4 mm, 8 mm). The inset shows the 8-mm hole punched in the center of one sensor. (d) The increase in resistance after punching holes of different sizes.

To further investigate how the size of the holes affected the resistance of the composite paper, we punctured composite samples with punches of different diameters. Figures 6c,d demonstrate that punches with small diameter (0.5 mm, 1 mm, 2 mm) induced small increases in resistance (~500 Ω). In contrast, subsequent punches of large diameters (4 mm, 8 mm) caused significant increases in resistance (~1850 Ω, ~6900 Ω, respectively). Compared with the 2-mm holes, 4-mm holes cause a 4-fold increase in resistance, while the 8-mm holes cause a 14-fold increase, indicating that our composite paper was capable of detecting, assessing, and classifying damage. The analytical model and numerical simulation verify that the resistance of the composite sheet increases nonlinearly with the hole size (Figures S14-S16).

3. Conclusion

This work demonstrates a scalable foam-laying and embossing method to fabricate cellulose-based conductive composite paper with tunable electrical properties. The conductivity of the nanocomposites increased nonlinearly with the concentration of CB, which followed universal scaling law from the percolation theory but with different critical exponents. Embossing the composite paper increased its conductivity and caused a maximum change of ~300 fold at the percolation threshold (3.8 wt%, or 0.36 vol%). Our composite paper showed stable piezoresistive responses within a broad pressure range from 1 kPa up to 5.5 MPa for 800 cycles.

This piezoresistive composite paper functioned as a tunable platform for creating capacitive and resistive sensors through embossed patterns, showing promise in applications for skin-like sensing for touch and pressure, intelligent packaging protection, and fabrication of other flexible electronics. The increasing resistance of the material during the damaging process has the potential to detect and assess the impact on applied surfaces, monitor structural health of buildings and vehicles, and alert people of danger. Overall, this work presents a potentially scalable process for manufacturing sheets of uniform porous composite paper with

tunable electrical conductivity and piezoresistivity, adaptable for new applications on flexible substrates.

4. Experimental Section

4.1 The process of making composite paper

(1) Preparation of aqueous dispersions of NBHK fibers

Uniform dispersion of the conductive filler in the cellulosic matrix is essential to achieving reproducible electrical properties. We used northern bleached hardwood kraft pulp (NBHK) (Prime C, Woodland Pulp LLC) as the matrix material and carbon black Vulcan XC-72R (Cabot Corporation) as the conductive filler. We first disintegrated/agitated a pulp-water suspension (consistency of 1.6%) by a kitchen blender for 3 minutes. After the agitation, the mean width and mean length-weighted length of fibers were approximately 18.9 μm and 762 μm, respectively (measured by MorFi fiber analyzer, Pulp and Paper Services, LLC, Figure S17).

(2) Preparation of aqueous dispersions of NBHK fibers and CB

We mixed the agitated pulp suspension with carbon black at an acceleration of ~70 g (686 m/s^2) in a resonant acoustic mixer (RAM, ResodynTM Acoustic Mixers, Inc) for 2 minutes to obtain a uniform slurry. We prepared composites consisting of 1 wt% to 40 wt% carbon black based on the dry weight in the ambient environment, as shown in Figure 2a. We did not go beyond 40 wt% as the conductivity started to level off at high concentrations.

(3) Preparation of CB-NBHK foam by adding SDS

We diluted the slurry with water to 0.26% consistency (4 g fiber/1.5 L water) and agitated it at 1000 rpm by a mechanical mixer for 3 minutes. Next, we added 0.4 g of sodium dodecyl sulfate (SDS, L4509, Sigma Aldrich) to the slurry, stirring it at 1700 rpm for 15 minutes to entrain air for a stable foam, as shown in Figure S1a. The final air content was around 70%.

(4) Preparation of CB-NBHK paper

We decanted the foam via a funnel onto a nylon mesh in a handsheet former with a diameter of 160 mm. To obtain compact structure and uniform surfaces, we covered the foam with a polished steel plate and applied vacuum filtration (88 KPa) for 3 minutes to dewater and filter the bubbles. (Figure S1b-d). We dried the sheet of composite paper in a drying ring for one day in the ambient environment.

4.2 Morphology observation

We examined the morphology of the prepared composite paper by a scanning electron microscope (SEM, Zeiss Sigma FESEM). We coated the samples with a 20-nm gold layer (Sputter Coater, Model EMS150T ES) and observed them under the conditions of high vacuum at an accelerating voltage of 5 kV.

4.3 Porosity calculation

The porosity, the ratio of pore volume to total volume, depends on the density of the composite. We deduced porosity by the theoretical composite density ρ_{ct} (the effective solid density by the combination of the filler and the cellulose), and the experimentally determined density ρ_{ce} (mass divided by volume) as Eq. (2) and Eq. (3) show.[53,54]

$$\phi = \left(1 - \frac{\rho_{ce}}{\rho_{ct}}\right) \times 100\% \quad (2)$$

$$\rho_{ct} = \frac{1}{\sum_{i=1}^{n}\left(\frac{W_i}{\rho_i}\right)} = \left(\frac{W_f}{\rho_f} + \frac{W_m}{\rho_m}\right)^{-1} \quad (3)$$

where the density of fillers is $\rho_f = \rho_{CB}$ =1.8g/cm^3 and the density of the matrix is $\rho_m = \rho_{cellulose\ fiber}$ =1.5g/cm^3.

4.4 Electrical characterization

We prepared U-shaped samples by a laser cutter (Versa VLS 2.3) and compressed the samples (Figure S1e) by a hydraulic press (maximum force of 88 kN, Series 3393, Carver Inc.). Before electromechanical characterization, we conditioned the samples in an environmental chamber for 24 hours to achieve the same moisture content within each (Figure S1f). The environmental conditions were 23°C and 50% relative humidity (RH) according to TAPPI Standard

T402. We compressed the legs of samples to reduce contact resistance during measurement. Then we measured the samples in the environmental chamber by clamping the compressed legs of the samples with a test fixture (HP14047) as shown in Figures S1g,h. By the admittance spectroscopy method (monitoring the admittance over a wide frequency range),[55] we characterized eight samples of each concentration of composite paper using an HP4192A LF impedance analyzer with a frequency range of 5 Hz to 13 MHz at an oscillator (OSC) level of 1V. From the two components of admittance (conductance *G*, and susceptance *B*), we calculated the AC conductivity σ,[56] impedance magnitude $|Z|$, and phase of the sample θ_Z according to Eq. (4) -Eq. (6).

$$\sigma(\omega) = |Y(\omega)|\frac{L}{A} = \sqrt{G(\omega)^2 + B(\omega)^2}\,\frac{L}{Wt} \quad (4)$$

$$|Z| = |R + jX| = \frac{1}{|Y|} = \frac{1}{|G+jB|} = \frac{1}{\sqrt{G^2+B^2}} \quad (5)$$

$$\theta_Z = -\tan^{-1}\left(\frac{X}{R}\right) = -\tan^{-1}\left(\frac{B}{G}\right) \quad (6)$$

where conductivity σ, admittance *Y*, conductance *G*, and susceptance *B* are functions of angular frequency (ω). Length *L*, width *W*, and thickness *t* are geometric parameters of the sample. The effective length of our U-shaped samples is 0.79 inch, calculated by COMSOL simulations shown in Figure S18.

4.5 Characterization of piezoresistive behavior

To characterize the piezoresistive behaviors of our composite paper, we carried out compression tests using an Instron machine 4411 with a 500-N load cell at 0.02 mm/s at room temperature and 50% RH. We embossed and clamped the two lateral edges of U-shaped samples (Figure S9d), between copper foil for electrical conduction. Then we exerted cyclic pressure by controlling displacement on the unembossed region (0.4 in×0.3 in) and recorded the force and electrical resistance simultaneously. In processing the data, we synchronized the data of pressure and resistance by aligning the peaks and rescaling the machine times. By interpolation, we obtained resistance data according to the range of pressure.

ASSOCIATED CONTENT

Supporting Information.

Picture of paper making, samples, picture of testing in an environmental chamber(Figure S1); SEM images of Composite paper before and after compression(Figure S2); Magnified SEM images of foam paper of different CB concentrations before and after compression(Figure S3); Average conductivity of composite paper at 10kHz before and after compression (Table S1); Comparison of the electrical conductivity of carbon-black composite paper (Table S2); Comparison of composite paper at 1 wt%, 1.4 wt%, 2 wt%, and 2.7 wt% concentration from 8 samples (Figure S4); Comparison of composite paper at 7.5 wt%, 10.5 wt%, and 14.6 wt% concentration from 8 samples (Figure S5); Comparison of composite paper at 20.5 wt%, 28.6 wt%, and 40 wt% concentration from 8 samples (Figure S6); Further analysis of conductivity with CB concentration beyond percolation threshold (Figure S7); Comparison of composite paper curve fitting of conductivity of composite paper at a concentration of CB less than the percolation threshold (Figure S8); Pressure sensitivities of composite paper during loading and unloading at pressure ranges of 1 kPa-250kPa and >250kPa (Table S3); Pressure sensitivities of composite paper during loading and unloading at pressure range of 1 kPa-50kPa (Table S4); Comparison of some pressure sensor (Table S5); Pressure-response of 7.5 wt% composite paper over time interval of 250 s, pressure-response of 7.5 wt% composite paper over time interval of 5 s, pressure-response curves for composite paper at pressure range (1 kPa-50 kPa), a prepared sample for piezoresistive tests. (Figure S9); Setup for shooting darts into the dartboard (Figure S10); Average increase in resistance of Rings 1-4 after the first and second shots at the dartboard (Figure S11); Electrical potential changes of a 0.5-mm thick plate with 2-mm holes to model darts (Figure S12); FEA simulation results of resistance change of composite sheet caused by darts in seven tests (Figure S13); A simplified model of a square plate with a hole for the punctured composite paper (Figure S14); Electrical potential changes

of a 0.5-mm thick plate with holes in diameter D ranging from 0 mm to 12 mm (Figure S15); Resistance change of punctured composite paper verse the radius of the hole by experiment, simulation, and analytical calculation (Figure S16); Optical images of cellulosic fibers taken by MorFi fiber analyzer (Figure S17); Effective length of samples determined by COMSOL simulation (Figure S18).

Demonstration of capacitive sensors fabricated by conductive foam paper (Video S1); Demonstration of using embossed conductive foam paper as a dartboard to detect damage and impact (Video S2).

The following files are available free of charge.

Supporting Information (PDF)

Video S1, S2 (MP4)

AUTHOR INFORMATION

Corresponding Author

Aaron D. Mazzeo, aaron.mazzeo@rutgers.edu, Department of Mechanical and Aerospace Engineering, Rutgers University, Piscataway, NJ 08854.

Author Contributions

T.L., X.Z., and A.D.M. designed the research; T.L., X.Z., R. K. P, J. X., J.L., M.A., W.G., C.C., and A.D.M. performed the research; T.L., X.Z., and A.D.M. analyzed the data. The manuscript was written through contributions of all authors. All authors have given approval to the final version of the manuscript. T.L. ‡ and X.Z. ‡ contributed equally.

Funding Sources

The authors acknowledge funding from the National Science Foundation Award Nos. 1610933 and 1653584, and the 2015−2016 GAIA grant from Rutgers, and support from the School of

Engineering and the Honors College of Rutgers. T.L. and X.Z. acknowledge fellowships from the China Scholarship Council. M.K.A. acknowledge funding from Rutgers Aresty Research Program.

ACKNOWLEDGMENT

The authors thank Prof. Jerry Scheinbeim for permitting the use of an impedance analyzer from his lab. The authors also thank Professor Fernando J. Muzzio for permitting the use of the Resodyn resonant acoustic mixers in his lab. The authors thank Andrew Kamp, Emily Zee, Anthony Castellano, Elias Bull, Jack Chiu, Colby Saxton, and Yunjian Cui in helping with the experiments.

ABBREVIATIONS

CB, carbon black; CNTs, carbon nanotubes; SEM, scanning electron microscope; RAM, Resonant Acoustic Mixer; SDS, sodium dodecyl sulfate; LCBC, low-concentration CB composites; HCBC, high-concentration CB composites; GUI, graphic user interface; NBHK, northern bleached hardwood kraft.

REFERENCES

(1) Lin, Y.; Gritsenko, D.; Liu, Q.; Lu, X.; Xu, J. Recent Advancements in Functionalized Paper-Based Electronics. *ACS Appl. Mater. Interfaces* **2016**, *8* (32), 20501–20515.

(2) Liang, T.; Zou, X.; Mazzeo, A. D. A Flexible Future for Paper-Based Electronics. In *Micro- and Nanotechnology Sensors, Systems, and Applications VIII*; International Society for Optics and Photonics, 2016; Vol. 9836, p 98361D.

(3) Li, R.-Z.; Hu, A.; Zhang, T.; Oakes, K. D. Direct Writing on Paper of Foldable Capacitive Touch Pads with Silver Nanowire Inks. *ACS Appl. Mater. Interfaces* **2014**, *6* (23), 21721–21729.

(4) Tao, L.-Q.; Zhang, K.-N.; Tian, H.; Liu, Y.; Wang, D.-Y.; Chen, Y.-Q.; Yang, Y.; Ren, T.-L. Graphene-Paper Pressure Sensor for Detecting Human Motions. *ACS Nano* **2017**, *11* (9), 8790–8795.

(5) Hyun, W. J.; Secor, E. B.; Rojas, G. A.; Hersam, M. C.; Francis, L. F.; Frisbie, C. D. All-Printed, Foldable Organic Thin-Film Transistors on Glassine Paper. *Adv. Mater.* **2015**, *27* (44), 7058–7064.

(6) Fujisaki, Y.; Koga, H.; Nakajima, Y.; Nakata, M.; Tsuji, H.; Yamamoto, T.; Kurita, T.; Nogi, M.; Shimidzu, N. Transparent Nanopaper-Based Flexible Organic Thin-Film Transistor Array. *Adv. Funct. Mater.* **2014**, *24* (12), 1657–1663.

(7) Gaspar, D.; Martins, J.; Bahubalindruni, P.; Pereira, L.; Fortunato, E.; Martins, R. Planar Dual-Gate Paper/Oxide Field Effect Transistors as Universal Logic Gates. *Adv. Electron. Mater.* **2018**, *4* (12), 1800423.

(8) Hamedi, M. M.; Ainla, A.; Güder, F.; Christodouleas, D. C.; Fernández-Abedul, M. T.; Whitesides, G. M. Integrating Electronics and Microfluidics on Paper. *Adv. Mater.* **2016**, *28* (25), 5054–5063.

(9) Lien, D.-H.; Kao, Z.-K.; Huang, T.-H.; Liao, Y.-C.; Lee, S.-C.; He, J.-H. All-Printed Paper Memory. *ACS Nano* **2014**, *8* (8), 7613–7619.

(10) Rattanarat, P.; Dungchai, W.; Cate, D.; Volckens, J.; Chailapakul, O.; Henry, C. S. Multilayer Paper-Based Device for Colorimetric and Electrochemical Quantification of Metals. *Anal. Chem.* **2014**, *86* (7), 3555–3562.

(11) Noviana, E.; P. McCord, C.; M. Clark, K.; Jang, I.; S. Henry, C. Electrochemical Paper-Based Devices: Sensing Approaches and Progress toward Practical Applications. *Lab. Chip* **2019**, *20* (1), 9–34.

(12) Lang, A. W.; Österholm, A. M.; Reynolds, J. R. Paper-Based Electrochromic Devices Enabled by Nanocellulose-Coated Substrates. *Adv. Funct. Mater.* **2019**, *29* (39), 1903487.

(13) Oh, H.; Kwak, S. S.; Kim, B.; Han, E.; Lim, G.-H.; Kim, S.-W.; Lim, B. Highly Conductive Ferroelectric Cellulose Composite Papers for Efficient Triboelectric Nanogenerators. *Adv. Funct. Mater.* **2019**, *29* (37), 1904066.

(14) Yang, P.-K.; Lin, Z.-H.; Pradel, K. C.; Lin, L.; Li, X.; Wen, X.; He, J.-H.; Wang, Z. L. Paper-Based Origami Triboelectric Nanogenerators and Self-Powered Pressure Sensors. *ACS Nano* **2015**, *9* (1), 901–907.

(15) Wang, Y.; Guo, H.; Chen, J.; Sowade, E.; Wang, Y.; Liang, K.; Marcus, K.; Baumann, R. R.; Feng, Z. Paper-Based Inkjet-Printed Flexible Electronic Circuits. *ACS Appl. Mater. Interfaces* **2016**, *8* (39), 26112–26118.

(16) Xin, Z.; Yan, M.; Gu, L.; Liu, J.; Liu, R.; Li, L.; Fang, Y.; Mo, L.; Li, Y.; Shen, Y.; Guolin, X.; Li, M.; Yang, L. Scalable Fabrication of Conductive Lines by Patterned Wettability-Assisted Bar-Coating for Low Cost Paper-Based Circuits. *Adv. Mater. Interfaces* **2019**, *6* (10), 1802047.

(17) Mazzeo, A. D.; Kalb, W. B.; Chan, L.; Killian, M. G.; Bloch, J.-F.; Mazzeo, B. A.; Whitesides, G. M. Paper-Based, Capacitive Touch Pads. *Adv. Mater.* **2012**, *24* (21), 2850–2856.
(18) Nassar, J. M.; Cordero, M. D.; Kutbee, A. T.; Karimi, M. A.; Sevilla, G. A. T.; Hussain, A. M.; Shamim, A.; Hussain, M. M. Paper Skin Multisensory Platform for Simultaneous Environmental Monitoring. *Adv. Mater. Technol.* **2016**, *1* (1), 1600004.
(19) Jung, M.; Kim, K.; Kim, B.; Cheong, H.; Shin, K.; Kwon, O.-S.; Park, J.-J.; Jeon, S. Paper-Based Bimodal Sensor for Electronic Skin Applications. *ACS Appl. Mater. Interfaces* **2017**, *9* (32), 26974–26982.
(20) Sadri, B.; Goswami, D.; Sala de Medeiros, M.; Pal, A.; Castro, B.; Kuang, S.; Martinez, R. V. Wearable and Implantable Epidermal Paper-Based Electronics. *ACS Appl. Mater. Interfaces* **2018**, *10* (37), 31061–31068.
(21) Liao, X.; Zhang, Z.; Liao, Q.; Liang, Q.; Ou, Y.; Xu, M.; Li, M.; Zhang, G.; Zhang, Y. Flexible and Printable Paper-Based Strain Sensors for Wearable and Large-Area Green Electronics. *Nanoscale* **2016**, *8* (26), 13025–13032.
(22) Zou, X.; Chen, C.; Liang, T.; Xie, J.; Gillette-Henao, E.-N.; Oh, J.; Tumalle, J.; Mazzeo, A. D. Paper-Based Resistive Networks for Scalable Skin-Like Sensing. *Adv. Electron. Mater.* **2018**, *4* (8), 1800131.
(23) Xu, H.; Fei Lu, Y.; Xin Xiang, J.; Kun Zhang, M.; Jin Zhao, Y.; Ying Xie, Z.; Ze Gu, Z. A Multifunctional Wearable Sensor Based on a Graphene/Inverse Opal Cellulose Film for Simultaneous, in Situ Monitoring of Human Motion and Sweat. *Nanoscale* **2018**, *10* (4), 2090–2098.
(24) Zhan, Z.; Lin, R.; Tran, V.-T.; An, J.; Wei, Y.; Du, H.; Tran, T.; Lu, W. Paper/Carbon Nanotube-Based Wearable Pressure Sensor for Physiological Signal Acquisition and Soft Robotic Skin. *ACS Appl. Mater. Interfaces* **2017**, *9* (43), 37921–37928.
(25) Koehly, R. Fabrication of Sustainable Resistive-Based Paper Touch Sensors: Application to Music Technology. Ph.D., McGill University (Canada), Canada, 2011.
(26) Zhang, J.; Lee, G.-Y.; Cerwyn, C.; Yang, J.; Fondjo, F.; Kim, J.-H.; Taya, M.; Gao, D.; Chung, J.-H. Fracture-Induced Mechanoelectrical Sensitivities of Paper-Based Nanocomposites. *Adv. Mater. Technol.* **2018**, *3* (3), 1700266.
(27) Gong, S.; Schwalb, W.; Wang, Y.; Chen, Y.; Tang, Y.; Si, J.; Shirinzadeh, B.; Cheng, W. A Wearable and Highly Sensitive Pressure Sensor with Ultrathin Gold Nanowires. *Nat. Commun.* **2014**, *5* (1), 3132.
(28) Gao, L.; Zhu, C.; Li, L.; Zhang, C.; Liu, J.; Yu, H.-D.; Huang, W. All Paper-Based Flexible and Wearable Piezoresistive Pressure Sensor. *ACS Appl. Mater. Interfaces* **2019**, *11* (28), 25034–25042.
(29) E. Anderson, R.; Guan, J.; Ricard, M.; Dubey, G.; Su, J.; Lopinski, G.; Dorris, G.; Bourne, O.; Simard, B. Multifunctional Single-Walled Carbon Nanotube –Cellulose Composite Paper. *J. Mater. Chem.* **2010**, *20* (12), 2400–2407.
(30) Dang Luong, N.; Pahimanolis, N.; Hippi, U.; T. Korhonen, J.; Ruokolainen, J.; Johansson, L.-S.; Nam, J.-D.; Seppälä, J. Graphene /Cellulose Nanocomposite Paper with High Electrical and Mechanical Performances. *J. Mater. Chem.* **2011**, *21* (36), 13991–13998.
(31) Hamedi, M. M.; Hajian, A.; Fall, A. B.; Håkansson, K.; Salajkova, M.; Lundell, F.; Wågberg, L.; Berglund, L. A. Highly Conducting, Strong Nanocomposites Based on Nanocellulose-Assisted Aqueous Dispersions of Single-Wall Carbon Nanotubes. *ACS Nano* **2014**, *8* (3), 2467–2476.
(32) Wang, F.; Drzal, L. T. The Use of Cellulose Nanofibrils to Enhance the Mechanical Properties of Graphene Nanoplatelets Papers with High Electrical Conductivity. *Ind. Crops Prod.* **2018**, *124*, 519–529.

(33) B. Dichiara, A.; Song, A.; M. Goodman, S.; He, D.; Bai, J. Smart Papers Comprising Carbon Nanotubes and Cellulose Microfibers for Multifunctional Sensing Applications. *J. Mater. Chem. A* **2017**, *5* (38), 20161–20169.
(34) Xiang, W.; Filpponen, I.; Saharinen, E.; Lappalainen, T.; Salminen, K.; Rojas, O. J. Foam Processing of Fibers As a Sustainable Alternative to Wet-Laying: Fiber Web Properties and Cause–Effect Relations. *ACS Sustain. Chem. Eng.* **2018**, *6* (11), 14423–14431.
(35) Sato, H.; Sano, M. Characteristics of Ultrasonic Dispersion of Carbon Nanotubes Aided by Antifoam. *Colloids Surf. Physicochem. Eng. Asp.* **2008**, *322* (1), 103–107.
(36) Romyen, N.; Thongyai, S.; Praserthdam, P. Surfactant-Dispersed Carbon Black in Polyimide Nanocomposites: Spectroscopic Monitoring of the Dispersion State in the Polymer Matrix. *J. Appl. Polym. Sci.* **2010**, *115* (3), 1622–1629.
(37) Jiang, L.; Wang, W.; Guan, A.; Wu, G. Heterocoagulation Behavior of Carbon Black with Surface Encapsulation through Emulsion Polymerization. *J. Appl. Polym. Sci.* **2016**, *133* (23).
(38) Nechita, P.; Năstac, S. Foam-Formed Cellulose Composite Materials with Potential Applications in Sound Insulation. *J. Compos. Mater.* **2018**, *52* (6), 747–754.
(39) Al-Qararah, A. M. Aqueous Foam as the Carrier Phase in the Deposition of Fibre Networks, University of Jyväskylä, 2015.
(40) Taya, M. *Electronic Composites: Modeling, Characterization, Processing, and MEMS Applications*; Cambridge University Press: New York, NY, USA, 2005.
(41) Nakamura, S.; Saito, K.; Sawa, G.; Kitagawa, K. Percolation Threshold of Carbon Black-Polyethylene Composites. *Jpn. J. Appl. Phys.* **1997**, *36* (8R), 5163.
(42) Nan, C.-W.; Shen, Y.; Ma, J. Physical Properties of Composites Near Percolation. *Annu. Rev. Mater. Res.* **2010**, *40* (1), 131–151.
(43) Pelíšková, M.; Piyamanocha, P.; Prokeš, J.; Varga, M.; Sáha, P. The Electrical Conductivity of Ethylene Butyl-Acrylate/Carbon Black Composites: The Effect of Foaming on the Percolation Threshold. *Synth. Met.* **2014**, *188*, 140–145.
(44) Cataldi, P.; Bayer, I. S.; Bonaccorso, F.; Pellegrini, V.; Athanassiou, A.; Cingolani, R. Foldable Conductive Cellulose Fiber Networks Modified by Graphene Nanoplatelet-Bio-Based Composites. *Adv. Electron. Mater.* **2015**, *1* (12), 1500224..
(45) Liu, H.; Huang, W.; Gao, J.; Dai, K.; Zheng, G.; Liu, C.; Shen, C.; Yan, X.; Guo, J.; Guo, Z. Piezoresistive Behavior of Porous Carbon Nanotube-Thermoplastic Polyurethane Conductive Nanocomposites with Ultrahigh Compressibility. *Appl. Phys. Lett.* **2016**, *108* (1), 011904.
(46) Huang, H.; Su, S.; Wu, N.; Wan, H.; Wan, S.; Bi, H.; Sun, L. Graphene-Based Sensors for Human Health Monitoring. *Front. Chem.* **2019**, *7*, 399.
(47) Mannsfeld, S. C. B.; Tee, B. C.-K.; Stoltenberg, R. M.; Chen, C. V. H.-H.; Barman, S.; Muir, B. V. O.; Sokolov, A. N.; Reese, C.; Bao, Z. Highly Sensitive Flexible Pressure Sensors with Microstructured Rubber Dielectric Layers. *Nat. Mater.* **2010**, *9* (10), 859–864.
(48) Mohammad Haniff, M. A. S.; Muhammad Hafiz, S.; Wahid, K. A. A.; Endut, Z.; Wah Lee, H.; Bien, D. C. S.; Abdul Azid, I.; Abdullah, M. Z.; Ming Huang, N.; Abdul Rahman, S. Piezoresistive Effects in Controllable Defective HFTCVD Graphene-Based Flexible Pressure Sensor. *Sci. Rep.* **2015**, *5* (1), 14751.
(49) Luheng, W.; Tianhuai, D.; Peng, W. Influence of Carbon Black Concentration on Piezoresistivity for Carbon-Black-Filled Silicone Rubber Composite. *Carbon* **2009**, *47* (14), 3151–3157.

(50) Matthews, N.; Hagmann, M. J.; Mayer, A. Comment: "Generalized Formula for the Electric Tunnel Effect between Similar Electrodes Separated by a Thin Insulating Film" [J. Appl. Phys. 34, 1793 (1963)]. *J. Appl. Phys.* **2018**, *123* (13), 136101.
(51) Kang, T.-K. Tunable Piezoresistive Sensors Based on Pencil-on-Paper. *Appl. Phys. Lett.* **2014**, *104* (7), 073117.
(52) Ding, T.; Wang, L.; Wang, P. Changes in Electrical Resistance of Carbon-Black-Filled Silicone Rubber Composite during Compression. *J. Polym. Sci. Part B Polym. Phys.* **2007**, *45* (19), 2700–2706.
(53) Agarwal, B. D.; Broutman, L. J.; Chandrashekhara, K. *Analysis and Performance of Fiber Composites*, 3rd ed.; John Wiley & Sons, 2017.
(54) Sehaqui, H.; Morimune, S.; Nishino, T.; Berglund, L. A. Stretchable and Strong Cellulose Nanopaper Structures Based on Polymer-Coated Nanofiber Networks: An Alternative to Nonwoven Porous Membranes from Electrospinning. *Biomacromolecules* **2012**, *13* (11), 3661–3667.
(55) Mabrook, M. F.; Petty, M. C. Effect of Composition on the Electrical Conductance of Milk. *J. Food Eng.* **2003**, *60* (3), 321–325.
(56) Sandler, J. K. W.; Kirk, J. E.; Kinloch, I. A.; Shaffer, M. S. P.; Windle, A. H. Ultra-Low Electrical Percolation Threshold in Carbon-Nanotube-Epoxy Composites. *Polymer* **2003**, *44* (19), 5893–5899.